

Approximating a gene regulatory network from non-sequential data

Cliff Stein*, Pratik Worah†

February 26, 2025

Abstract

Given non-sequential snapshots from instances of a dynamical system, we design a compressed sensing based algorithm that reconstructs the dynamical system. We formally prove that successful reconstruction is possible under the assumption that we can construct an approximate clock from a subset of the coordinates of the underlying system.

As an application, we argue that our assumption is likely to be true for RNA-seq datasets, and thus we can recover the underlying nuclear receptor networks and predict pathways, as opposed to genes, that may differentiate between interesting phenotypes in some publicly available datasets.

1 Introduction

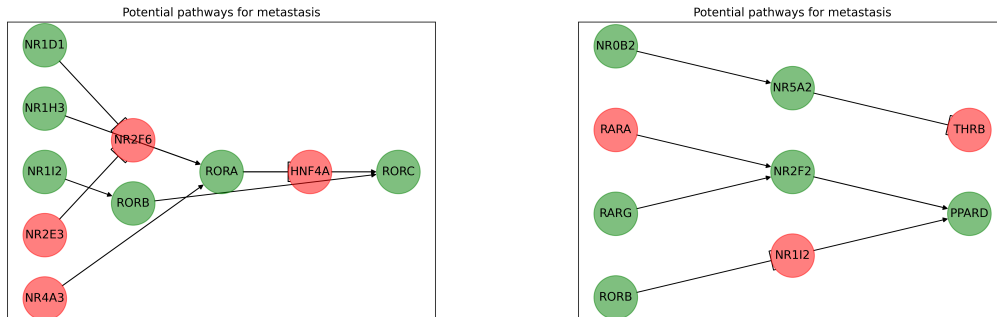
The problem of reconstructing a noisy linear dynamical system from sequential observations to predict its next step is a basic problem in filtering theory. In this paper, we consider the case when the order of observations has been lost, i.e., they are not necessarily sequential. Such a situation arises often in biological samples, where although one can collect information about cells, it is impossible to know perfectly where the cells are in their cell cycle relative to each other. Another area where this problem arises is in reconstructing a linear system learnt over noisy networks, for example in a noisy financial feed where the packets may be disordered or dropped.

Our theoretical contributions: We formulate a concrete version of the above reconstruction problem and solve it under the assumptions discussed in Subsection 1.3. Algorithm 1 in Section 3 is our main algorithmic contribution and Theorem 4.1 in Section 4 upper-bounds the error of the recovered dynamical system using Algorithm 1. The compressed sensing methods used in our paper ensure that reconstruction can be successful, even with small sample sizes, under sparsity assumptions.

Application to genomics: We also show an application of our algorithm to genomic datasets (see Subsection 1.1 for details). We use the reconstructed linear dynamical systems to compute genomic pathways that are prominently different between pathological and reference samples. Thus, unlike standard tools, such as Love et al. [2014], that predict genes whose expressions may differentiate between two phenotypes, we can predict pathways that differentiate between two phenotypes. Figure 1, based on the breast cancer RNA-seq dataset [Cancer Genome Atlas Network: Daniel C Koboldt et al, 2012], represents our main contribution in this context.

*Columbia University and Google Research

†NYU and Google Research (pworah@cims.nyu.edu)



(a) Potential pathways for metastasis. The pathological "phenotype" is presence of metastasis while the reference is absence of metastasis. (b) Potential pathways which may be adverse to longer survival. The pathological "phenotype" is survival below 12months while reference is survival beyond 60months.

Figure 1: Predicted pathways where gene $A \rightarrow$ gene B means that A (indirectly) up-regulates B , while the flat arrowhead indicates (indirect) down-regulation. A green node indicates that the corresponding gene expression positively correlates with the pathological phenotype (eg. metastasis), while a red node indicates positive correlation with the reference phenotype. Based on the figure, one prominent pathway could be: NR1I2 up-regulates RORB which up-regulates RORC, whose increased expression is positively correlated with metastasis; based on data in Cancer Genome Atlas Network: Daniel C Koboldt et al [2012]. See Section 6 for details on how Algorithm 3 was used to recover the pathways from the breast cancer dataset Cancer Genome Atlas Network: Daniel C Koboldt et al [2012].

1.1 Application to genomics

We apply Algorithm 1 to the transcriptional regulation problem in genomics. An important problem in genomics is to understand transcriptional regulation – which genes directly regulate a given gene. For example, one version of the problem is to reconstruct Gene Regulatory Networks (GRNs) from gene expression snapshots measured using RNA-seq data. The surveys Badia-i Mompel et al. [2023] and Barbuti et al. [2020] cover the tools and techniques employed in the study of GRNs. In this paper, we model the dynamical system underlying gene expression as a Markov process. Such models have been used to study gene regulation before (see for example Kepler and Elston [2001] and Chu et al. [2017]). The paper Kepler and Elston [2001] gives a detailed overview of modeling transcription regulation by stochastic differential equations (SDEs); and the Ornstein-Uhlenbeck process that we employ in this paper is just a linear approximation of such SDE models that is analytically tractable and yet expressive enough to capture first order behavior. To the best of our knowledge, we are not aware of prior work that uses ℓ_1 optimization to reconstruct GRNs or the underlying Markov processes.

1.2 Our contribution

Using Algorithms 1, 2 and 3, and the publicly available RNA-seq dataset [Cancer Genome Atlas Network: Daniel C Koboldt et al, 2012], we have predicted pathways, restricted to nuclear receptors (for computational tractability reasons). We show these results in Figure 1 and observe that they may distinguish between metastatic and non-metastatic breast cancers. See Sections 3.1 and 6 for

details.

Note that we do not have the resources to verify the results experimentally, but our predictions may help guide other researchers by narrowing down the genes and pathways for experiments. One way to verify the predictions would be to run our algorithms on a variety of malignant vs control (RNA-seq) datasets and find pathways that are common among the malignant samples. Among the common pathways, one can check for genes that are targets of known drugs. If such drugs exist and are known to be effective, then they help verify the predictions of our algorithms. Conversely, any genes shared amongst common predicted pathways, that are not yet known, can also be used as targets for newer drugs. In other words, our ideas should be applicable to the design of basket trials, where physicians aim to identify and target the same gene or mutation even though they may be treating different cancers. Having a prediction of the underlying pathways may help narrow the number of interesting gene targets that need be explored for therapies. Such trials have been critical in discovering novel therapies like anti-PD1 therapies (for e.g. Le et al. [2017]).

1.3 Underlying assumptions and verification

Our algorithms, specifically Algorithm 1, rely on three assumptions: (1) sparsity: the rows of the matrix,¹ are zero (or near zero) in most entries, (2) a mean field model assumption: the expressions in the RNA-seq data-set represent an “average” cell in the tissue concerned, and (3) existence of an approximate clock: we should be able to (roughly) order our cell samples according to cell age (measured as time since last cell division). We now justify these assumptions.

First, the sparsity assumption is expected to hold for GRNs because the transcriptional regulation of a given gene directly relies on only a handful of polymerases, promoters and previous gene products (see, for example Kepler and Elston [2001]). Even if we replace direct regulation by downstream regulation within a few steps, for example when studying GRNs restricted to nuclear receptor genes only, we still expect the resulting matrix to be sparse.

Second, we assume that the population weighted mean expression of any given gene in the tissue sample, that is reflected in the RNA-seq expression value for that gene, is a good approximation of the gene expression in the tissue. Such an assumption is made in mean field theories. The mean field model is usually a valid approximation of a dynamical system when: (a) the sample size is large and (b) fluctuations in value are small (c.f. the Ginzburg criterion). That fluctuations should be small, i.e., the variance for a given gene expression should be small, is intuitive, because biological systems are usually in equilibrium (homeostasis). For an organism to be able to maintain equilibrium, large fluctuations in gene expression should be a rare occurrence, as successfully reverting the system back near its mean is harder to do from far flung outlier values. So if the sample size is large enough, then the mean field assumption should be valid.

Finally, before justifying the approximate clock assumption, we first discuss the reason we assume the existence of an approximate clock. We work with RNA-seq data, which is more readily available, unlike single-cell RNA-seq data. In single-cell RNA-seq data, it is possible to order cells by their latent time (see for example HKU single cell workshop [2021]). However, for RNA-seq data, latent time is not available, as latent time is a model-based construct. One saving grace is that *our algorithms do not use the cell sample ordering except to reconstruct the covariance matrix of increments, which is a pretty robust to noise*, in that it is only significantly effected if the

¹This is the matrix that constitutes of the coefficients of the first order (degree 1) terms in the linearization of the underlying dynamical system.

approximate ordering used has too many errors. Therefore, using appropriate cyclin expression levels to order cell samples in readily available RNA-seq data, although noisy, is sufficiently accurate for our purposes; as evidenced by our verification on a couple of single cell RNA-seq datasets (see Figures 3 and 5).

To elaborate, we verify that the reconstructed covariance matrix of increments is indeed robust to a small number of errors in ordering that may arise from using an *approximate* clock in three different ways: (1) theoretical justification: we prove that the reconstructed covariance matrix is correct as long as the approximate clock meets certain formal assumptions (Theorem 4.1), (2) by simulation in Section 5: we use synthetic data to study the error in the reconstructed covariance matrix as function of the number of errors in the approximate clock (Figure 2), and (3) by comparing the approximate ordering based on cyclin expressions with the ordering based on cell latent time in murine pancreatic single cell RNA-seq dataset from Bastidas-Ponce et al. [2019] (Figure 3) and murine dentate gyrus dataset of Hochgerner et al. [2018] (Figure 5). In each case, we find that the covariance matrix computed using the approximate clock will be close to the actual covariance matrix.

2 Related problems

Related problems in genomics Our approximate cyclin based ordering problem is related to the problem of trajectory inference, which has been well explored in single cell RNA-seq literature [Saelens, W. and Cannoodt, R. and Todorov, H. et al., 2019]. Trajectory inference is likely a harder problem to solve, because we only need to order cell samples well enough to approximately recover a specific covariance matrix in our algorithms, but in the trajectory inference problem one needs to order the cell samples in the correct sequence to predict cellular development.

Finally, it is possible that cyclin expressions themselves may be effected in many situations by the pathology under consideration (see for e.g. Ghafouri-Fard et al. [2022]). In such cases, our algorithms can not be applied directly with cyclins to construct the approximate clock, but it may be possible to use a different set of gene expressions related to cell division, upstream from cyclins, that are verified to be not effected by the pathology, to construct the approximate clock, on a case by case basis.

Related problems in filtering From an abstract algorithmic perspective, the line of work closest to our problem is the Kalman filtering problem in the presence of network loss and delays (see Li et al. [2021], Liu et al. [2020] and Nikfetrat and Esfanjani [2019], and the references therein). However, such results typically assume a independent identical probability of packet drop or delay, sometimes modelled by a Markov process of interest. Also, although the idea of computing conditioned Gaussian distributions (for the error upper-bound in Theorem 4.1) is similar to that used for the analysis of the Kalman filter, the problem studied in our paper differs from the standard filtering problem: (1) we are interested in recovering the underlying linear system and not in predicting the next step of the system, and (2) we use sparsity critically in our algorithms.

2.1 Organization

In Section 3, we formulate the problem and describe our algorithms based on the approximate clock. Next, we verify the existence of an approximate clock is enough to reconstruct the underlying GRN; first theoretically in Section 4 and then empirically in Subsections 5.1 and 5.2. Finally, we give more details on how we obtain the breast cancer pathways in Figure 1 in Section 6.

3 Problem statement and overview

Definition 3.1. (see for example Oksendal [2013]) Suppose we have a n -dimensional Ornstein-Uhlenbeck (OU) process

$$dx_t = Bx_t dt + AdW_t, \quad (1)$$

where W_t is n -dimensional standard Brownian motion, A is the *diffusivity* matrix, AA^T is the *covariance matrix of increments*, and B the *drift* matrix.

Suppose that we observe x_t at various time points in $[0, T]$ for large T , but we either do not have the ordering information or do not keep the samples ordered. Thus the covariance matrix of the increments of x_t is not assumed to be known in this paper, since it requires ordering information for its computation. Then, we want to know whether we can recover the underlying (unknown) $n \times n$ drift matrix B , that characterizes our dynamical system.²

Remark 3.2. If we are given an ordering of x_t s (correct or with errors) as $(x_{t_0}, x_{t_1}, \dots, x_{t_n})$ then we may compute covariance matrix of increments, with respect to that ordering, as the average $\frac{1}{n} \sum_{k=1}^n (x_{t_k} - x_{t_{k-1}})^T (x_{t_k} - x_{t_{k-1}})$. If $t_0 \leq t_1 \leq \dots \leq t_n$ then AA^T is the empirical covariance matrix of increments and is closely approximated by the average, by Sanov type concentration theorems (See Dembo and Zeitouni [2010]). Moreover, being an average, this matrix is fairly robust to noise and small errors; a fact that we will use critically in this paper.

In general, reconstructing B without ordering information of the x_t may not be possible. However, the main technical result in this paper shows that if: (1) there exists an "approximate clock" (see Definition 3.3) and (2) B is row sparse, i.e., most of the entries in each row of B are zero or close to zero; then we can approximately reconstruct B with few samples in polynomial time, by solving a convex program.

Definition 3.3. Given an OU process as in Equation 1, we say that there exists an *approximate clock* if we know that some non-empty subset of the n coordinates (of x_t), or some projection of the process, has a positive drift in each coordinate, and the trace of the diffusivity matrix of the process is smaller than all the drift coordinates.³

To keep the presentation simple, we will assume that if there exists a single coordinate of $x(t)$,⁴ denoted by $\tau(t)$, and it is modeled by the diffusion:

$$d\tau(t) = \delta dt + \varepsilon dW'_t, \quad (2)$$

²We have assumed the system is centered about 0 but that is not an issue since the long term average can be computed without knowing the ordering and subtracted from the observations.

³The idea being that the clock process is likely to be increasing for most finite length time intervals.

⁴Here we assume a single coordinate exists as opposed to multiple coordinates or allowing a linear combination of coordinates

where W_t' is standard Brownian motion and δ is positive and much greater than ε^2 ; then $x(t)$ is said to admit an approximate clock.⁵

Assuming B is row sparse, i.e., each row of B has only $s = \log^{O(1)}(n)$ non-zero entries, and the number of samples t is larger than $s \log(n)$, and the existence of an approximate clock; our *main algorithmic contribution* is Algorithm 1, that can approximately reconstruct B from the t samples.

We will use the approximate clock to recover an approximation of the matrix A , which we denote by \tilde{A} . We won't actually need \tilde{A} but rather the covariance of the increments: $\tilde{A}\tilde{A}^T$; and in Theorem 4.1 in Section 4, we show that ordering the x_i values using $\tau(t)$ and computing the covariance from the increments closely approximates the covariance of the increments computed using the ordering based on the actual time.

Algorithm 1 runs in polynomial time as the main steps are computing a covariance matrix and solving the convex optimization problem in Step 1 of Algorithm 1, which is a second order cone program. This convex optimization is a slight variation of basis pursuit in the compressed sensing literature (see for example Foucart and Rauhut [2013]) and therefore unique reconstruction is guaranteed under sparsity assumptions. In particular the following uniqueness theorem holds true for the matrix \tilde{B} recovered by Algorithm 1.

Theorem 3.4. *Dirksen et al. [2018]* Let s denote the row sparsity of B , i.e., each row has at most s non-zero coordinates, then for $m = \Omega(\log n)$ large and the sample times $\{t_1, \dots, t_m\}$ for samples $\{x_{t_1}, \dots, x_{t_m}\}$ are uniformly distributed, then with probability $1 - o(1)$ (for large n): $\|\tilde{B} - B\|_1 = 0$, i.e., B can be recovered uniquely by solving a convex program. If however, the rows are not exactly s sparse and the ℓ_1 norm of the $n - s$ remaining entries in any row is at most ϵ , then we have: $\|\tilde{B} - B\|_1 \leq \epsilon n$.

While the proof follows by easy modifications of known results in existing compressed sensing literature (see Foucart and Rauhut [2013] or Dirksen et al. [2018]), we note the one novelty here over existing compressed sensing literature: the formulation of the constraint in Step 1 of Algorithm 1 uses the characterization of the long term variance of the OU process (see Oksendal [2013]).

Algorithm 1 recovers the drift matrix B from the covariance matrix Σ and the (approximate) covariance matrix of the increments $\tilde{A}\tilde{A}^T$ up to an additive factor (that is just the ratio of diffusivity over drift of the approximate clock).

Algorithm 1 Recover dynamical system

- 1: **Input:** Unordered snapshots $\{x_1, \dots, x_t \in \mathbb{R}^n; t \in [0, T]\}$ derived from an Ornstein-Uhlenbeck process $dx_t = Bx_t dt + AdW_t$; where the diffusivity matrix A is known up to a constant additive error as \tilde{A} , and B is row sparse but unknown.
 - 2: **Output:** A recovered matrix \tilde{B} that is close (in ℓ_1 norm) to B .
 - 3: **Algorithm starts:**
 - 4: Compute the $n \times n$ covariance matrix of the random vectors $\{x_1, \dots, x_t\}$, denoted Σ
 - 5: \triangleright Note:(1) computing Σ does not require ordering the x_i s
 - 6: \triangleright (2) $B(i, \cdot)$ denotes the i^{th} row of B
 - 7: Solve $\tilde{B} := \arg \min_B \sum_{i=0}^n \|B(i, \cdot)\|_2$ s.t. $\Sigma B + B^T \Sigma = -\frac{\tilde{A}\tilde{A}^T}{2}$
 - 8: return \tilde{B}
-

⁵Notation: We use x_t and $x(t)$ interchangeably.

Remark 3.5. Note that the only use of ordering using approximate clock is to recover the matrix $\tilde{A}\tilde{A}^T$ in Algorithm 1, we do not use the ordering information anywhere else.

Often it is not enough to recover the drift matrix, but we need to distinguish one linear system from another, where the first is a small perturbation of the second, and one has only few samples of the second at hand. This exact case happens for genomic data samples, where one system is the reference and many samples are available, but another system is some rare genetic condition or disease for which fewer samples are available. Algorithm 2 obtains the *perturbation matrix* P (within a small error) that distinguishes the second linear system from the first. Note that the algorithm always returns a value for a large enough choice of the noise parameter η and small enough choice of ϵ in Step 2 of Algorithm 2, since that will suffice to make the convex program feasible. Hence we chose a small enough η (via binary search) that just makes the convex program feasible.

Algorithm 2 Order and recover perturbations between two dynamical systems

- 1: **Input:** Unordered snapshots $\{x_1, \dots, x_t \in \mathbb{R}^n; t \in [0, T]\}$ and $\{x'_1, \dots, x'_{t'} \in \mathbb{R}^n; t' \in [0, T']\}$ derived from two Ornstein-Uhlenbeck processes $dx_t = Bx_t dt + AdW_t$ and $dx'_t = B'x'_t dt + A'dW_t$; where the diffusivity matrices A and A' are known up to small error, but B and B' are unknown. Moreover, $t' \ll t$ and B and B' are row sparse.
 - 2: **Output:** A recovered matrix \tilde{B} that is close to B in ℓ_1 norm, and a perturbation matrix \tilde{P} such that $\tilde{B} + \epsilon\tilde{P} \simeq B'$, for a small positive parameter ϵ .
 - 3: **Algorithm starts:**
 - 4: Use Algorithm 1 to compute \tilde{B}
 - 5: \triangleright The smaller number of samples prevents direct computation of \tilde{B}' , so we compute a first order approximation.
 - 6: Compute the $n \times n$ covariance matrix of the random vectors $\{x'_1, \dots, x'_{t'}\}$, denoted Σ'
 - 7: \triangleright Choose a small noise η so that the following convex program program is feasible
 - 8: \triangleright Note: P_{ij} denotes the i^{th} row, j^{th} column element of matrix P
 - 9: Solve $\tilde{P} := \arg \min_P \sum_{i,j=0}^n |P_{ij}|$ s.t. $\|(\Sigma - \Sigma')\tilde{B}^T + \tilde{B}(\Sigma - \Sigma') - \epsilon(\Sigma'P^T + P\Sigma')\|_2 \leq \eta$
 - 10: return \tilde{P}
-

3.1 Algorithm for isolating genomic pathways

As a concrete application, we use the recovered perturbation matrix \tilde{P} to isolate the paths consisting entirely of high weight edges in the directed graph (defined below) underlying the dynamical system, since these paths should reflect the prominent genomic pathways that differentiate the reference dynamical system from the pathological dynamic system. We note that more standard methods like time series analysis based on Fourier transform of the recovered linear system can also be tried out, but our method below is far simpler, and thus probably more robust to recovery errors, and it suffices to illustrate the pathways that can be recovered.

The matrix P can be thought of as a directed graph with entry P_{ij} reflecting a weighted directed edge from the node corresponding to gene j to that for gene i . A *prominent* path is defined to be one such that all its edges have weight higher than some fixed threshold, say θ . For such a prominent path p to potentially reflect an actual underlying genetic pathway that promotes the pathological phenotype, one of the following intuitive conditions should hold:

1. If the gene corresponding to the terminal node of p positively correlates with the pathological

phenotype then it should be up-regulated by the gene preceding it in the path p ; moreover, the same property or property (2) should now hold for the subpath terminating in the penultimate gene, and so on.

2. Otherwise, if the gene corresponding to the terminal node of p negatively correlates with the pathological phenotype then it should be down-regulated by the gene preceding it in the path p ; moreover, the same property or property (1) should now hold for the subpath terminating in the penultimate gene, and so on.

This intuition leads to Algorithm 3 which predicts prominent genomic pathways that may be experimentally verified to confirm that some or all of them lead to the pathological phenotype.

Algorithm 3 Recover Pathways

- 1: **Input:** The underlying linear dynamical systems matrices \tilde{B} and \tilde{B}' and the correlations between each of the coordinates (corresponding to genes) and the two phenotypes of interest.
 - 2: **Output:** A set of pathways of a given length L that are prominently different between the two phenotypes.
 - 3: \triangleright **Algorithm starts:**
 - 4: Compute and sort the list of genes in descending order in terms of the absolute value of their correlation coefficient with the pathological phenotype, denote this list as \vec{g}
 - 5: Compute $C := \text{Diag}(\vec{g})(\tilde{B}' - \tilde{B})$
 - 6: Fix a positive threshold θ and set $C_{ij} = 0$ if $C_{ij} < \theta$, denote the resulting matrix as Π_θ
 - 7: Compute the set of paths of length L in the graph with adjacency matrix Π_θ and return them.
-

The results of running Algorithm 3 on the breast cancer dataset [Cancer Genome Atlas Network: Daniel C Koboldt et al, 2012] to isolate critical differentiating pathways are described in Figure 1. In this figure, we show predicted pathways where gene A \rightarrow gene B means that A (indirectly) up-regulates B, while the flat arrowhead indicates (indirect) down-regulation. A green node indicates that the corresponding gene expression positively correlates with the pathological phenotype (metastasis), while a red node indicates positive correlation with the reference phenotype (cancer without metastasis). We predict potential pathways, restricted to nuclear receptors, for metastasis. Based on Figure 1(a), one prominent pathway could be: NR1I2 up-regulates RORB which up-regulates RORC. A simple correlation coefficient analysis of RNA-seq data in Cancer Genome Atlas Network: Daniel C Koboldt et al [2012] shows that the expression of RORC is positively correlated with metastasis. However, the actual role of RORC in metastasis is likely to be far more complicated (see Oh et al. [2016]).

4 Theoretical bounds on error from an approximate clock

In this section, we derive an upper-bound on the error of the recovered diffusivity matrix when we use an approximate clock. We will assume that our dynamical system can be modeled by an OU process and it has a coordinate, or a linear combination of coordinates, that admit a positive drift which is larger than the diffusivity. This coordinate will act as an approximate clock. Theorem 4.1 shows that if we use this approximate clock then the recovered diffusivity is not too different from the diffusivity that would be obtained if we knew the ordering in the dynamical system.

Theorem 4.1. *Assuming that the clock coordinate $\tau(t)$ is independent of the remaining coordinates of x_t , the diffusivity matrix $\tilde{A}\tilde{A}^T$ computed using the approximate clock $\tau(t)$ is asymptotically equal to the actual diffusivity, i.e.,*

$$\tilde{A}\tilde{A}^T = \lim_{h \rightarrow 0} \mathbb{E} \left[\frac{1}{\delta T} \int_0^T \langle (x(\tau(t+h)) - x(\tau(t))), (x(\tau(t+h)) - x(\tau(t))) \rangle d\tau(t) \right] \simeq AA^T, \quad (3)$$

for $\varepsilon \ll \delta$.⁶

The proof is deferred to the supplement (Section A.1). If the correlations between the randomness in $\tau(t)$ and other coordinates are significant then we can evaluate Equation 12 as follows.

Lemma 4.2. *Let $\rho \in \mathbb{R}^{1 \times n}$ be the covariance matrix between W'_t and W_t , which are the Brownian motions in the definitions of $\tau(t)$ and x_t respectively; then the quadratic variation below evaluates as:*

$$\mathbb{E} [\langle AdW_\tau, Bx(\tau)d\tau \rangle] = \varepsilon A \rho x(t)^T B^T dt. \quad (4)$$

The proof follows immediately from the definition of quadratic variation. Therefore, following a similar proof as Theorem 4.1, the error to $\tilde{A}\tilde{A}^T$ from Theorem 4.1 is changed by an additive factor that is $O(\varepsilon \max_{i,j} \{\rho_{ij}\})$. So when all coordinates of $\varepsilon \rho$ are small, the characterization of $\tilde{A}\tilde{A}^T$ in Theorem 4.1 continues to hold.

5 Empirical bounds on error from an approximate clock

Theorem 4.1 shows that the covariance matrix AA^T in Algorithm 1 is determined by an approximate clock as long as $\frac{\varepsilon}{\delta}$ is small. In this section we verify the same fact empirically.

5.1 Empirical verification using synthetic data

First, we use synthetic data to plot the error in determining the matrix AA^T , i.e., $AA^T - \tilde{A}\tilde{A}^T$, as a function of the number of errors in the cell sample orderings. Note that the latter decreases as $\frac{\varepsilon}{\delta} \rightarrow 0$. In Figure 2, we plot the Frobenius norm of $AA^T - \tilde{A}\tilde{A}^T$ as a function of the number of errors (equal to the number of inversions) in ordering.

In order to generate the plot in Figure 2, we used an OU process with a 10×10 identity matrix as a stand-in for A ; we set $B := -Id + G$, where G is a random Gaussian matrix, and we used time-steps of size 0.0001 to generate the sample path for 1000 time-steps. We introduce k errors/inversions (the x coordinate in Figure 2) in the sample path by picking k pairs of points, uniformly at random, in the sample path and swapping the pairs. Finally, we compute the corresponding empirical covariance matrix: $\tilde{A}(k)\tilde{A}(k)^T$, from the perturbed path with k inversions, the corresponding Frobenius norm of $\tilde{A}(k)\tilde{A}(k)^T - AA^T$ and plot the latter as a function of k .

5.2 The approximate clock using single cell RNA-seq datasets

It can be argued that neither Theorem 4.1 nor Figure 2 uses cyclin expressions anywhere. Perhaps using cyclin expressions to order cells leads to a significantly large number of errors in cell sample

⁶Note: (1) Since $\mathbb{E}[\tau(t)] = \delta t$ the normalization of $\tilde{A}\tilde{A}^T$ has a δT term as opposed to a T term, (2) one can skirt around the issue of negative values of τ by assuming that $\tau(0)$ is large, that will ensure τ remains positive with high probability.

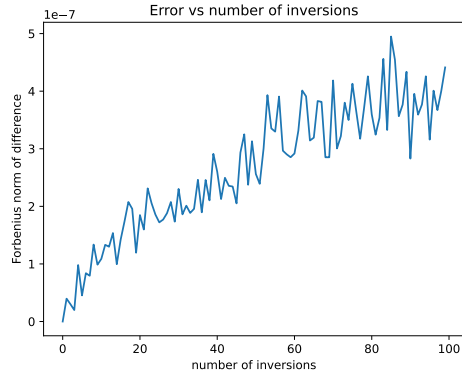


Figure 2: Error in determining covariance matrix as a function of the amount of error in the construction of the approximate clock. Note that the Frobenius norm of the difference is small and does not grow too quickly, and is close to zero near zero.

orderings of RNA-seq data. In this subsection, we allay that fear as well.

Yet another way to verify that the approximate clock using cyclin expressions does not lead to a large error in-between AA^T and $\tilde{A}\tilde{A}^T$ is to use single cell RNA-seq data. Such datasets admit an ordering of cell samples using latent time based on underlying RNA velocity models. In this subsection, we verify that AA^T (determined using latent time) and $\tilde{A}\tilde{A}^T$ (determined using a simple ordering using cyclin expressions) are close, based on single cell RNA-seq dataset from murine pancreatic tissue [Bastidas-Ponce et al., 2019].

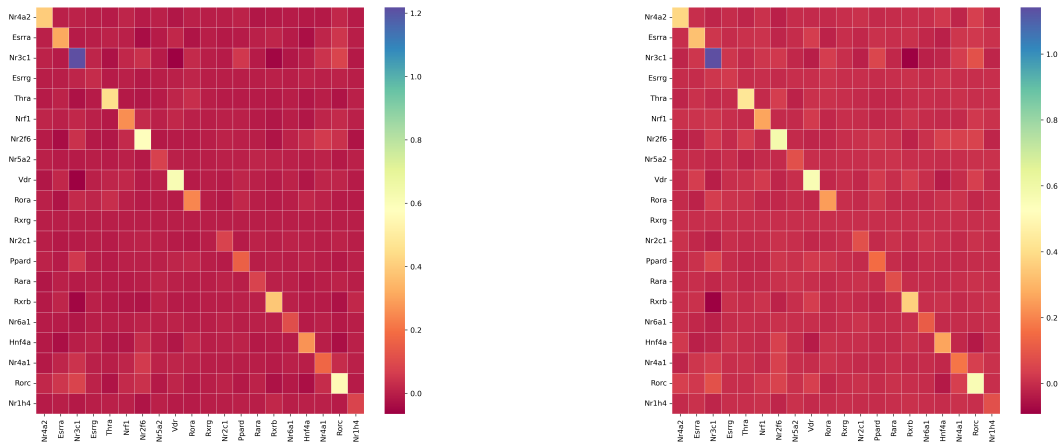
So we compute the covariance matrix of increments, among significantly expressed nuclear receptors in the murine pancreatic scRNA-seq dataset from [Bastidas-Ponce et al., 2019], in two ways:

1. First, we compute the matrix $\tilde{A}\tilde{A}^T$ using an approximate clock that involves ordering the cell samples by the difference in between two cyclin expressions, say Cyclins I and D, i.e., $\tau(c) := \text{Cyclin I} - \text{Cyclin D}$ for a given cell c . Cyclin I and D represent the optimal choice based on the correlations in Figure 3(d).
2. Next, we compute the matrix AA^T by using the latent time function in scVelo as our ordering (this is our ground truth).

We use the total RNA expression levels data for nuclear receptors in the five groups: alpha, beta, epsilon, pre-endocrine and ductal cells in the murine pancreatic single cell RNA-seq dataset [Bastidas-Ponce et al., 2019] for this purpose. Thus we obtain five instances of AA^T and five instances of $\tilde{A}\tilde{A}^T$.

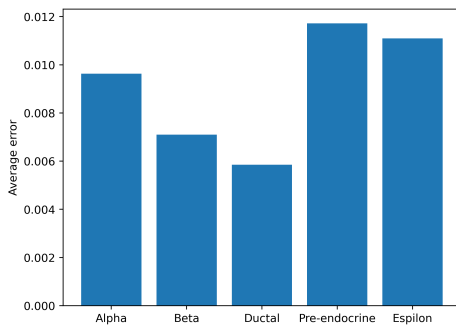
As can be seen in Figure 3(c), the error measured as the average of entry-wise absolute difference of the computed matrix i.e., $AA - \tilde{A}\tilde{A}^T$ is indeed small, much smaller than the variances (diagonals in the heatmaps), thus leading credence to our claim that *covariance matrices of increments are robust to few errors in sample orderings*.

We performed a similar analysis on the murine dentate gyrus dataset of Hochgerner et al. [2018]. The covariance matrices computed in two ways (using scVelo latent time and cyclin expression based ordering) are shown in Figure 5 in the supplement.

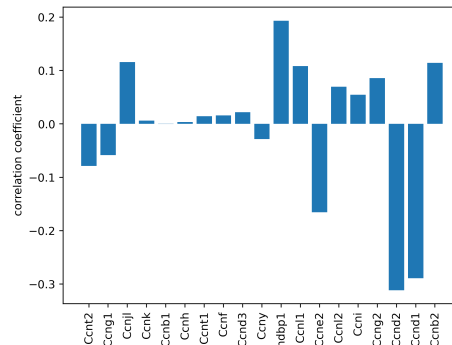


(a) Dynamical system obtained from latent time computation

(b) Dynamical system obtained from Cyclin clock



(c) Average entry-wise difference between the recovered dynamical system matrix for various cell clusters



(d) Correlations between cyclin expressions and scVelo latent time

Figure 3: Robustness of Cyclin clock in single cell pancreatic RNA-seq data

The covariance matrices thus computed are virtually identical, again demonstrating the effectiveness of the simple cyclin based ordering of samples, as far as computation of covariance matrices is concerned. Our next step is to demonstrate the use of these covariance matrices in the computation of pathways, in Figure 1, in the next section.

6 The reconstructed dynamical system from breast cancer data

Finally, in order to generate the pathways in Figure 1, we used the publicly available breast cancer dataset [Cancer Genome Atlas Network: Daniel C Koboldt et al, 2012]. The dataset consists of tumor and germline samples from 825 patients, including mRNA expression data for about 500 patients. We used this RNA-seq data as input to our algorithms. First, we used Algorithms 1

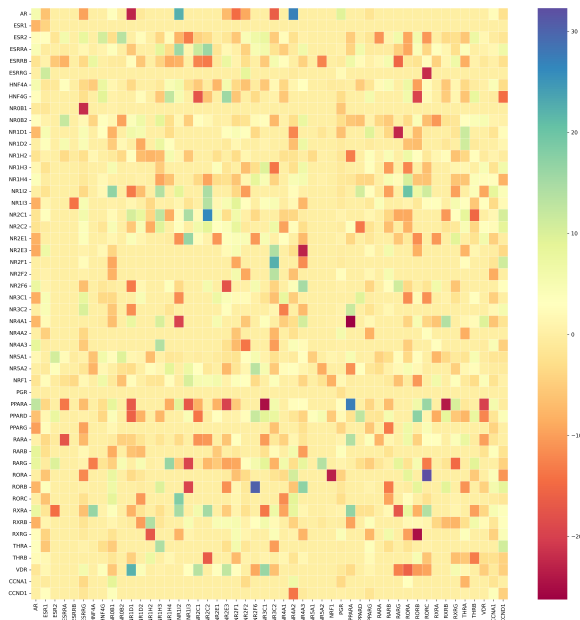


Figure 4: Perturbations of GRN towards metastasis. The matrix represents the first order approximation of changes in interaction between genes in presence of metastasis. Values far from 0 (yellow) represent a prediction that there is significant up or down regulation in an interaction between a given pair of genes.

and 2 to compute the underlying linear dynamical system matrix: \tilde{B} and the perturbations: \tilde{P} are shown in Figure 4 while the recovered dynamical system is shown in Figure 6 in the supplement. Since the dataset samples are unordered we use a linear combination of cyclin A and D expression levels, as our approximate clock, to order the data-points by cell age. Based on known literature about human cyclins, if we were to obtain a random sample of two cells from a tissue and found the difference, i.e., cyclin A - cyclin D levels, was relatively higher for sample 1 over sample 2 than we know that sample 1 was more advanced in the cell cycle than sample 2 (with some error). Thus we can use their difference in their expression as our approximate clock. Note that we can't verify how good this clock is, since we don't have access to any ground truth clock for Cancer Genome Atlas Network: Daniel C Koboldt et al [2012] dataset samples that orders cells by their relative cell cycle stage. We used Algorithm 3 on inputs \tilde{B} and \tilde{P} to obtain the pathways in Figure 1.

7 Conclusion

In conclusion, we have demonstrated the usefulness of ℓ_1 optimization methods to reconstruct the underlying GRNs using RNA-seq data from a breast cancer dataset. We suspect that our methods should be useful in the optimal design of basket trials in general. Due to lack of resources and

domain expertise we have not been able to verify the predictions ourselves. However, domain experts should be able to generate and verify such predictions to further their basic understanding of the genomic pathways underlying the conditions.

8 Acknowledgements

The authors are grateful to Dr. Jacob Glass and Prof. S.R.S. Varadhan for helpful discussion and comments.

References

- P. Badia-i Mompel, L. Wessels, S. Müller-Dott, R. Trimbour, R. O. Ramirez Flores, R. Argelaguet, and J. Saez-Rodriguez. Gene regulatory network inference in the era of single-cell multi-omics. *Nature Reviews Genetics*, 24:739–754, 2023.
- R. Barbuti, R. Guri, P. Milazzo, and L. Nasti. A survey of gene regulatory networks modelling methods: from differential equations, to Boolean and qualitative bioinspired models. *Journal of Membrane Computing*, 2:207–226, 2020.
- A. Bastidas-Ponce, L. D. Sophie Tritschler, K. Scheibner, M. Tarquis-Medina, C. Salinno, S. Schirge, I. Burtscher, A. Böttcher, F. J. Theis, H. Lickert, and M. Bakht. Comprehensive single cell mRNA profiling reveals a detailed roadmap for pancreatic endocrinogenesis. *Development*, 146(12):dev173849, 2019.
- Cancer Genome Atlas Network: Daniel C Koboldt et al. Comprehensive molecular portraits of human breast tumours. *Nature*, 490(7418):61–70, 2012.
- B. Chu, M. Tse, R. Sato, and E. Read. Markov State Models of gene regulatory networks. *BMC Systems Biology*, 11, 2017.
- A. Dembo and O. Zeitouni. *Large Deviations Techniques and Applications*. Springer-Verlag Berlin Heidelberg, 2010. doi: 10.1007/978-3-642-03311-7.
- S. Dirksen, G. Lecue, and H. Rauhut. On the gap between rip properties and sparse recovery conditions. *IEEE Transactions on Information Theory*, 64(8):5478–5487, 2018.
- S. Foucart and H. Rauhut. *A Mathematical Introduction to Compressive Sensing*. Birkhäuser New York, NY, 2013.
- S. Ghafouri-Fard, T. Khoshbakht, B. M. Hussen, P. Dong, N. Gassler, M. Taheri, A. Baniahmad, and N. A. Dilmaghani. A review on the role of cyclin dependent kinases in cancers. *Cancer Cell International*, 22, 2022.
- HKU single cell workshop. <https://statbiomed.github.io/SingleCell-Workshop-2021/RNA-velocity.html>, 2021.
- H. Hochgerner, A. Zeisel, P. Lonnerberg, and S. Linnarsson. Conserved properties of dentate gyrus neurogenesis across postnatal development revealed by single-cell rna sequencing. *Nature Neuroscience*, 21:290–299, 2018.
- T. B. Kepler and T. C. Elston. Stochasticity in transcriptional regulation: origins, consequences, and mathematical representations. *Biophysical journal*, 81:3116–3136, 2001.
- D. T. Le, J. N. Durham, K. N. Smith, H. Wang, B. R. Bartlett, L. K. Aulakh, S. Lu, H. Kemberling, C. Wilt, B. S. Luber, et al. Mismatch repair deficiency predicts response of solid tumors to PD-1 blockade. *Science*, 357(6349):409–413, 2017.
- H. Y. H. Li, Y. Xia, and L. Li. Distributed Kalman Filtering Over Sensor Networks With Transmission Delays. *IEEE Transactions on Cybernetics*, 51(11):5511–5521, 2021.

- D. Liu, Z. Wang, Y. Liu, and F. Alsaadi. Extended kalman filtering subject to random transmission delays: Dealing with packet disorders. *Information Fusion*, 60:80–86, 2020.
- M. Love, W. Huber, and S. Anders. Moderated estimation of fold change and dispersion for RNA-seq data with DESeq2. *Genome Biology*, 15(550), 2014.
- A. Nikfetrat and R. M. Esfanjani. Self-tuning Kalman filter for compensation of transmission delay and loss in line-of-sight guidance. *Proceedings of the Institution of Mechanical Engineers, Part G: Journal of Aerospace Engineering*, 233(11):4191–4201, 2019.
- T. G. Oh, S.-C. M. Wang, B. R. Acharya, J. M. Goode, J. D. Graham, C. L. Clarke, A. S. Yap, and G. E. Muscat. The Nuclear Receptor, ROR γ , Regulates Pathways Necessary for Breast Cancer Metastasis. *EBioMedicine*, pages 59–72, 2016.
- B. Oksendal. *Stochastic Differential Equations: An Introduction with Applications*. Springer, Berlin, 2013.
- Saelens, W. and Cannoodt, R. and Todorov, H. et al. A comparison of single-cell trajectory inference methods. *Nature Biotechnology*, 37:547–554, 2019.

A Supplement

A.1 Proof of Theorem 4.1

Proof. Note that

$$\tilde{A}\tilde{A}^T = \lim_{h \rightarrow 0} \mathbb{E} \left[\frac{1}{\delta T} \int_0^T \langle (x(\tau(t+h)) - x(\tau(t))), (x(\tau(t+h)) - x(\tau(t))) \rangle d\tau(t) \right] \quad (5)$$

by definition of x_t . By the tower property of conditional expectation and switching the order of integrals:

$$\mathbb{E} \left[\frac{1}{T} \int_0^T \langle dx(\tau(t)), dx(\tau(t)) \rangle \right] = \mathbb{E} \left[\frac{1}{T} \int_0^T \mathbb{E} \left[\langle dx(\tau(t)), dx(\tau(t)) \rangle \middle| \tau(t) \right] \right] \quad (6)$$

Recall that,

$$dx(t) = Bx(t)dt + AdW_t \quad (7)$$

$$d\tau(t) = \delta dt + \varepsilon dW'_t, \quad (8)$$

where W'_t and W_t are independent standard Brownian motions in \mathbb{R} and \mathbb{R}^n respectively. The inner conditional expectation can be evaluated in terms of $\tau(t)$ as follows:

$$\mathbb{E} \left[\langle dx(\tau(t)), dx(\tau(t)) \rangle \middle| \tau(t) \right] = \mathbb{E} \left[\langle Bx(\tau)d\tau + AdW_\tau, Bx(\tau)d\tau + AdW_\tau \rangle \middle| \tau(t) \right]. \quad (9)$$

Note that we are conditioning a Gaussian with another Gaussian, so the result is a Gaussian variable. The quadratic variation term in the RHS expectation is a sum of three types of terms that can be calculated using:

$$\mathbb{E} [\langle AdW_\tau, AdW_\tau \rangle] = AA^T d\tau(t) \quad (10)$$

$$\mathbb{E} [\langle Bx(\tau)d\tau, Bx(\tau)d\tau \rangle] = \varepsilon^2 Bx(\tau)x(\tau)^T B^T dt \quad (11)$$

$$\mathbb{E} [\langle AdW_\tau, Bx(\tau)d\tau \rangle] = 0. \quad (12)$$

The last equality follows because we have assumed that W'_t and W_t are independent. However, that covariance can be calculated explicitly as well, if needed.

Therefore,

$$\int_0^T \mathbb{E} \left[\langle dx(\tau(t)), dx(\tau(t)) \rangle \middle| \tau(t) \right] = \int_0^T (AA^T d\tau(t) + \varepsilon^2 Bx(\tau)x(\tau)^T B^T dt) . \quad (13)$$

Note that

$$\mathbb{E} \left[\frac{1}{\delta T} \int_0^T AA^T d\tau(t) \right] = \mathbb{E} \left[\frac{1}{T} \int_0^T AA^T dt \right], \quad (14)$$

since the integral with dW'_t is a martingale with zero mean. Therefore, if $\varepsilon \ll \delta$ then

$$\mathbb{E} \left[\frac{1}{\delta T} \int_0^T \langle dx(\tau(t)), dx(\tau(t)) \rangle \right] \simeq \frac{1}{T} \int_0^T AA^T dt. \quad (15)$$

□

A.2 Verification of reconstruction from scRNA-seq data for dentate gyrus Hochgerner et al. [2018]



(a) Dynamical system obtained from latent time computation

(b) Dynamical system obtained from Cyclin clock

Figure 5: Robustness of Cyclin clock in single cell dentate gyrus RNA-seq data (note that the other nuclear receptors were not well expressed hence were excluded)

A.3 Recovered GRN from RNA-seq data Cancer Genome Atlas Network: Daniel C Koboldt et al [2012]

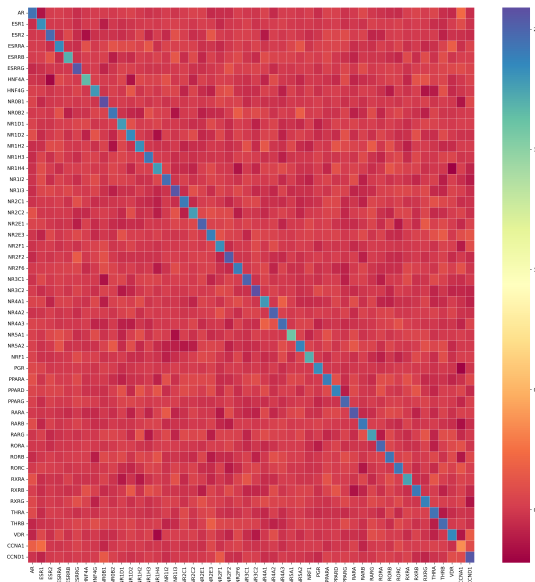


Figure 6: Underlying dynamical system for non-metastatic cases